For example, in a two-stage design, the primary sampling unit (PSU) is selected at the first stage. A PSU might be defined as a delineation of an SMU or a selected region such as a $10\,m \times 10\,m$ area. The secondary sampling units (SSUs) are selected from within the PSU. If much of the travel cost is involved in traveling to the PSU (for example, navigating to a selected delineation of an SMU), then selecting several SSUs from each PSU may be more cost effective than choosing one SSU from each PSU.

Choosing Efficient Design and Estimation Strategies

In the geostatistical literature, there has been some controversy over the applicability of classical survey sampling strategies in soil surveys. Many of the above design approaches have been investigated in the context of soil surveys [9, 10]. Choosing the appropriate combination of sample design and estimator was investigated for soil surveys in [4] and for general spatial sampling problems in [6].

References

[1] Abbitt, P.J. & Nusser, S.M. (1995). Sampling approaches for soil survey updates, *Proceedings of the American Statistical Association, Section on Statistics and the Environment*, American Statistical Association, Alexandria, pp. 87–91.

[2] Breidt, F.J. (1995). Markov chain designs for one-per-stratum sampling, *Survey Methodology* **21**, 63–70.

[3] Breidt, F.J. (1995). Markov chain designs for one-per-stratum spatial sampling, *Proceedings of the American Statistical Association, Section on Survey Research Methods*, Vol. 1, American Statistical Association, Alexandria, pp. 356–361.

[4] Brus, D.J. & de Gruijter, J.J. (1997). Random sampling or geostatistical modelling? Choosing between design-based and model-based sampling strategies for soil (with discussion), *Geoderma* **80**, 1–44.

[5] Burgess, T.M., Webster, R. & McBratney, A.B. (1981). Optimal interpolation and isarithmic mapping of soil properties IV. Sampling strategy, *Journal of Soil Science* **32**, 643–659.

[6] Cressie, N. & Aldworth, J. (1996). Spatial statistical analysis and its consequences for spatial sampling, in *Proceedings of the Fifth International Geostatistics Congress*, E. Baafi, ed., Kluwer, Dordrecht.

[7] de Gruijter, J.J. (1985). Transect sampling for reliable information on mapping units, in *Soil Spatial Variability, ISSS and SSSA*, PUDOC, Wageningen.

[8] Di, H.J., Trangmar, B.B. & Kemp, R.A. (1989). Use of geostatistics in designing sampling strategies for soil survey, *Soil Science Society of America Journal* **53**, 1163–1167.

[9] Domburg, P., de Gruijter, J.J. & Brus, D.J. (1994). A structured approach to designing soil survey schemes with prediction of sampling error from variograms, *Geoderma* **62**, 151–164.

[10] Domburg, P., de Gruijter, J.J. & van Beck, P. (1997). Designing efficient soil survey schemes with a knowledge-based system using dynamic programming, *Geoderma* **75**, 183–201.

[11] Food and Agriculture Organization of the UN (1972). Soil Fertility Survey and Research: The Philippines. Soil survey and land classification of the Penaranda river irrigation system area. United Nations Development Program, Rome.

[12] Landon, J.R. ed. (1984). *Booker Tropical Soil Manual*, Booker–Tate, London.

[13] McBratney, A.B. & Webster, R. (1983). Optimal interpolation and isarithmic mapping of soil properties V. Co-regionalization and multiple sampling strategies, *Journal of Soil Science* **34**, 137–162.

[14] McLaren, R.G. & Cameron, K.C. (1990). *Soil Science: An Introduction to the Properties and Management of New Zealand Soils*, Oxford University Press, Auckland.

[15] Nikol'skii, N.N. (1963). *Practical Soil Science*, Israel Program for Scientific Translation, Jerusalem.

[16] Revut, I.B. & Rode, A.A. eds (1969). *Experimental Methods of Studying Soil Structure*, Kolos, Leningrad.

[17] Soil Survey Division Staff (1993). *Soil Survey Manual*, USDA SCS, Handbook No. 18. `http://www.statlab.iastate.edu/soils/nssh/`.

[18] Steur, G.G.L. et al. (1961). Methods of soil surveying in use at the Netherlands soil survey institute, *Boor en Spade* **11**, 59–67.

[19] Thompson, S. (1992). *Sampling*, Wiley, New York.

[20] Webster, R. (1977). *Quantitative and Numerical Methods in Soil Classification and Survey*, Clarendon Press, Oxford.

[21] Webster, R. (1985). *Quantitative Spatial Analysis of Soil in the Field*, Vol. 3, Springer-Verlag, New York, Chapter 1.

(*See also* **Atmospheric dispersion: Basic**; **Line-transect sampling**; **Soil conservation and remediation**)

PAMELA J. ABBITT

Soil wetness index

Soil wetness is identified as the magnitude of liquid water residing in a vertical profile observable by

a satellite instrument. The frequencies flown on the SSMI (Special Sensor Microwave Imager [2]) instrument are incapable of penetrating into the soil or through a dense vegetative canopy. Therefore, the index represents the amount of water in the upper reaches of the soil (top few centimeters) or, where a dense canopy is present, it represents the water intercepted by the canopy. The index can also monitor the amount of liquid water present in a melting snow pack.

The SSMI instrument is flown by the US Defense Meteorological Satellite Program (DMSP) and contains 7 channels: four with vertical (V) polarization: 19, 22, 37, 85 GHz, and three with horizontal (H) polarization: 19, 37 and 85 GHz. These channels reside at window (19 and 37 GHz) and near window (22 and 85 GHz) wavelengths. Liquid water near the surface depresses the emissivity differently at the various wavelengths, and the relationship of these emissivity values is used to identify the amount of liquid water in each SSMI observation (Figure 1). Consequently the more water that is present near the surface, the greater emissivity is depressed in the lower frequencies and the larger the observed temperature gradient across the spectrum of microwave frequencies.

This relationship, denoted the Basist Wetness Index (BWI), has been used to identify the magnitude

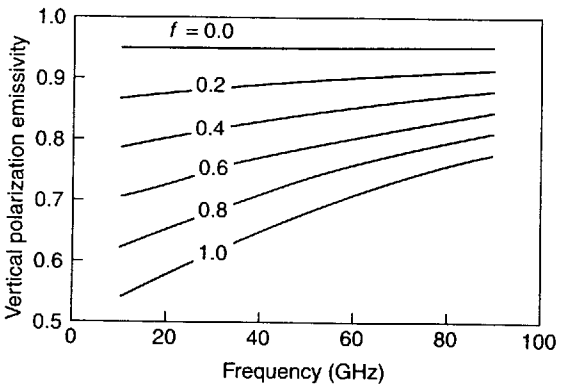

Figure 1 A theoretical relationship of emissivity over a spectrum of microwave frequencies for six different magnitudes of surface wetness. The top curve corresponds to 0% of the surface covered with water, and the bottom curve corresponds to 100% of the surface covered by water. Note the slope of the curve as the fractional amount of surface water increases. Reproduced from [2] by permission of the American Meteorological Society

of surface water. An example of the BWI is presented in Figure 2, and the numerical calculation of the index is defined below. The global map of the BWI values for July 1999 identifies the location of the Intertropical Convergence Zone over northern Africa, and shows the monsoonal areas in India and southeastern Asia. Some major river basins (*see* **Rivers, canals and estuaries**) around the world (i.e. Amazon, Congo, Rio Paraguay and Mississippi) are evident. Note that the major tributaries of the Amazon are also observed, but the dense surrounding forest does not appear wet, since the instrument cannot see through the dense canopy. The irrigated regions around numerous river valleys (e.g. Indus in Pakistan, Ganges in India, Red River in China) are also clearly detected. The highest values tend to correspond to the tundra regions, where the snow cover has melted and water has pooled on the surface, since the permafrost below will not allow the water to percolate through the soil. The areas with zero wetness correspond to the great deserts of the world.

One advantage of passive microwave observations is the ability to penetrate clouds. Unfortunately, the frequencies used in this study cannot penetrate a dense vegetative canopy, which limits their ability to see the ground [5]. As a result, it is difficult to determine what percentage of the signal comes from the vegetated canopy vs. the ground below [6]. Even when bare ground is observed at microwave frequencies, the available wavelengths cannot penetrate more than a few centimeters below the surface. Therefore, the microwave measurements do not always correspond to the true soil moisture [3]. The following section will identify regions of the world where the wetness index does correspond with upper level soil moisture, as well as areas where it does not.

Precipitation values were used as validation of the wetness index signal throughout many regions of the world. This analysis provided some clear distinctions where the BWI has utility and where the canopy or soil type limits its usefulness. Over most agricultural areas there is a strong correspondence between the BWI signal and precipitation. This is attributed to two factors. First, crops require sufficient quantities of soil moisture to flourish. Consequently, there is a strong signal for the satellite to detect. Second, agricultural practices generally require that the ground is plowed and the crops are grown in rows with exposed soil on the sides, allowing the satellite to gain sufficient

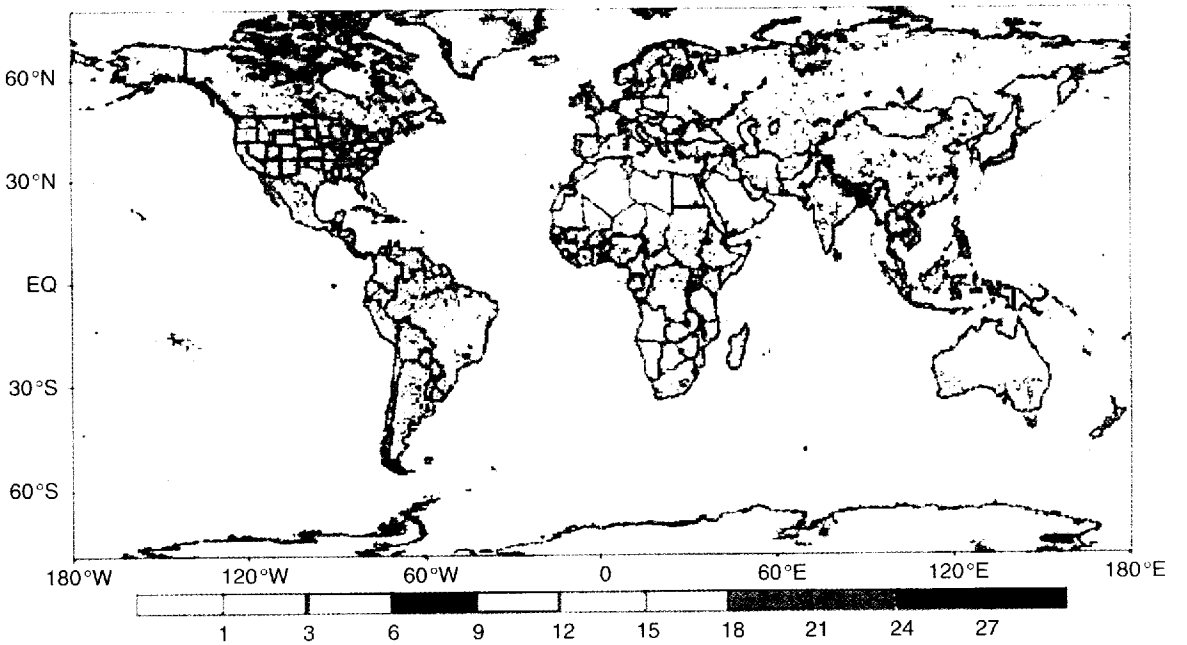

Figure 2 A map of the Basist Wetness Index (BWI) for the globe during the month of July 1999. Note the high values in the tundra, wet lands and broad river valleys. The moderate values correspond to areas where the radiating surface contains some water, while low values correspond to the major desert regions or dense vegetation that hides the ground from the satellite observation. Reproduced from [2] by permission of the American Meteorological Society

signal from the ground surface where precipitation regulates the quantity of upper level soil moisture. Over many agricultural areas around the world the wetness index has the best correspondence with precipitation values accumulated over a two- to three-month period. This result strongly implies that the BWI signal measures upper level soil moisture, which is regulated by precipitation over an extended period.

Conversely, the BWI does not show a reliable correspondence to precipitation or upper level moisture in heavily vegetated areas, including regions that are covered by a forest canopy and regions where foliage is sufficiently dense to block the wetness signal originating from the soil. In such cases most of the signal corresponds with canopy interception of precipitation. The BWI also has limited utility for loose granular soils. These tend to be sparsely vegetated areas and receive limited precipitation (although there are some areas of sandy soil where abundant vegetation and precipitation occur). Under such conditions the moisture does not reside near the surface. It either penetrates below the layer where the satellite receives a signal, or is rapidly evaporated.

Another aspect of the microwave signal is its ability to monitor melting snow cover. Melted snow is characterized by a strong 'wet' signature, but this signature can have little correlation with the amount of water entering the soil, particularly when a shallow snow pack melts during the day only to freeze again the following night [1, 4]. Thus it is imperative for the diurnal cycle of the meltwater to be monitored. If a wet signature is detected during both the morning and afternoon it is highly likely that the water is not refreezing during the night and has saturated the snow pack sufficiently that meltwater is steadily being released. Under this condition the magnitude of the BWI has a strong correspondence to the quantity of liquid water exiting the snow pack. Figure 3 demonstrates this signal by displaying the spatial structure of the BWI during April 1997. At this time above-average temperatures and rainfall rapidly melted the excessive snow pack, causing extensive flooding in the Red River Valley along the Minnesota and North Dakota border (*see* **Hydrological extremes**). The area of snow melt of northern US and southern Canada is also clear.

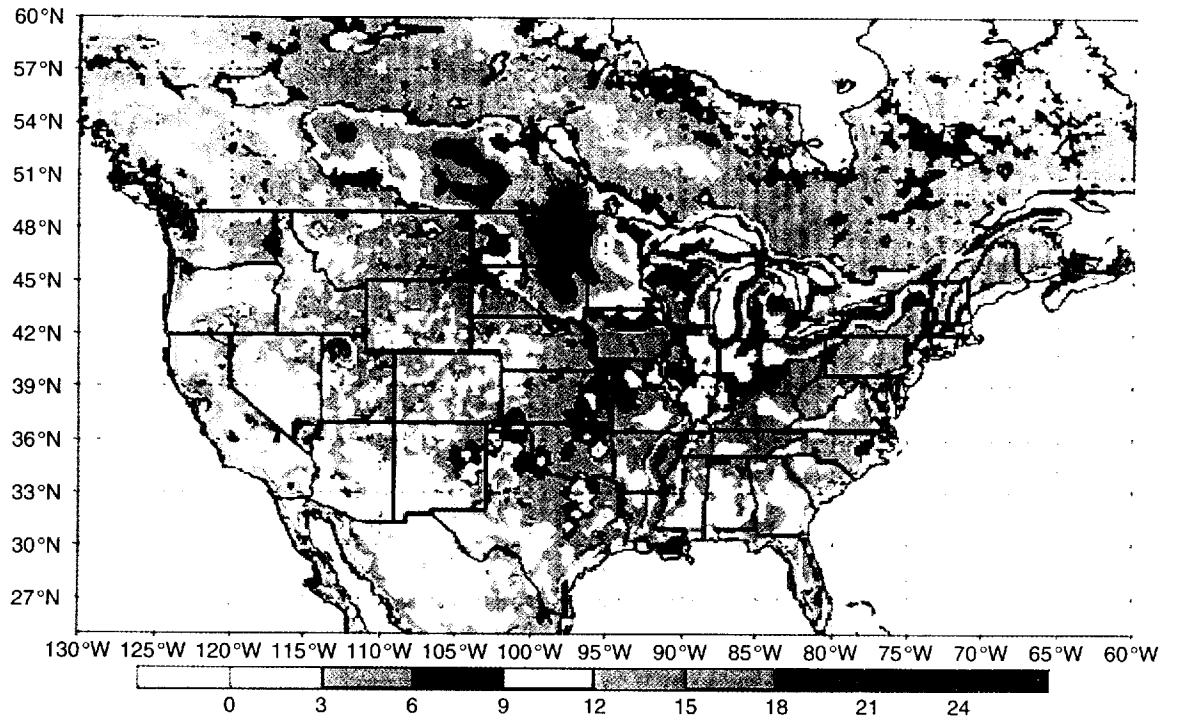

Figure 3 The percentage of the radiating surface that is liquid water for April 1997. Reproduced from [2] by permission of the American Meteorological Society

The BWI is defined by a statistical relationship that quantitatively identifies how emissivity at the various frequencies corresponds with the magnitude of liquid water near the surface. It takes the form of a linear relationship between channel measurements, i.e.

$$\begin{aligned} \mathrm{BWI} &= \Delta\varepsilon \times T_s \\ &= \beta_0[T_b(\nu_2) - T_b(\nu_1)] \\ &\quad + \beta_1[T_b(\nu_3) - T_b(\nu_2)] \end{aligned} \tag{1}$$

where $\Delta\varepsilon$ (change of emissivity) was empirically determined from global SSMI measurements, T_s is surface temperature over wet land, T_b is the satellite brightness temperature for a channel, ν_n is a frequency observed by the SSMI instrument, and each β_n is an empirically derived regression coefficient (*see* **Linear models**).

This relationship was calibrated from over 44 000 in situ temperatures observed at the surface near the time of the satellite overpass. The best relationship used four of the satellite's channel measurements from the SSMI observation. The majority of the weight (i.e. largest β term) corresponds to the 85 V channel – where the emissivity of water is highest. A histogram of the **residuals** (difference between in situ based and satellite-derived surface temperature over all the observations identified with a 'wet surface') is presented in Figure 4. These residuals between the SSMI derived temperature and the observed in situ temperature at the time of the satellite overpass peak near zero (average error is 0.021 °C), have a low standard deviation (2.64 °C), and are highly symmetrical (skewness is 0.066 °C). The atmospheric contribution has also been minimized by the relationship between window and water vapor channels (developed in the regression equation), although some error corresponds with atmospheric contamination. (For a more complete description of the procedure of calculating the emissivity effect of water in the radiating surface, see [7].) The difference between the 19 GHz (vertically polarized) channel measurement and the statistically derived surface temperature defines the

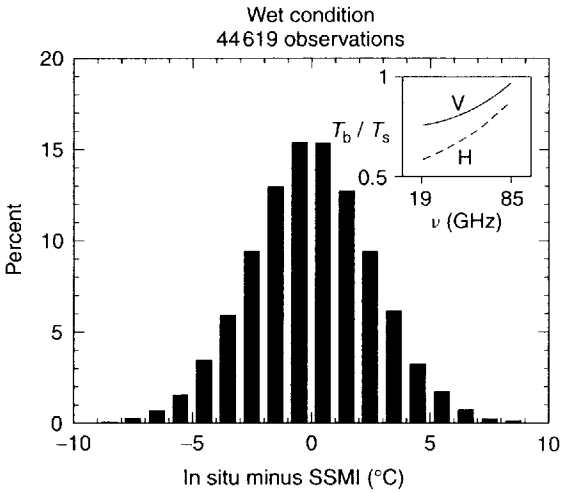

Figure 4 A histogram of the differences between in situ and SSM/I derived surface temperatures when wetness is detected on the surface. The right corner of the figure demonstrates how the observed temperature varies with frequency when surface water is present. As wetness increases, the observed temperature at the lower frequency becomes more depressed, which increases the slope of measurements across the SSMI frequencies. Reproduced from [2] by permission of the American Meteorological Society

BWI. Therefore the BWI is dynamically derived from each observation of every orbit. These derived values serve as the foundation of this study.

References

[1] Basist, A.N., Grody, N.C., Peterson, T.C. & Williams, C.N. (1998). Using the Special Sensor Microwave Imager to monitor land surface temperature, wetness, and snow cover, *Journal of Applied Meteorology* **37**, 888–911.

[2] Basist, A.N., Williams, C., Grody, N., Ross, T., Shen, S., Chang, A., Menne, M.J. & Ferraro, R. (2001). Using the Special Sensor Microwave Imager to monitor surface wetness, *Journal of Hydrometeorology* **3**, 297–308.

[3] Entekhabi, D., Nakamura, H. & Njoku, E.G. (1995). Solving the inverse problem for soil moisture and temperature profiles by sequential assimilation of multifrequency remotely sensed observations, *IEEE Transactions on Geoscience and Remote Sensing* **32**, 438–448.

[4] Matzler, C. (1994). Passive microwave signatures of landscapes in winter, *Meteorology and Atmospheric Physics* **54**, 241–260.

[5] Owe, M., van de Griend, A.A. & Chang, A.T.C. (1992). Surface moisture and satellite microwave observations in semiarid southern Africa, *Water Resources Research* **28**, 829–839.

[6] Wang, J.R. (1985). Effects of vegetation on soil moisture sensing from an orbiting microwave radiometer, *Remote Sensing of the Environment* **17**, 141–151.

[7] Williams, C., Basist, A., Peterson, T.C. & Grody, N. (1999). Calibration and validation of land surface temperature anomalies derived from the SSM/I, *Bulletin of the American Meteorological Society* **81**, 2141–2156.

(*See also* **Global environment monitoring system, water**; **Groundwater monitoring**; **National Resources Inventory (NRI), US**; **Remote sensing**; **Soil conservation and remediation**)

ALAN BASIST, CLAUDE WILLIAMS, NORMAN GRODY, THOMAS ROSS & SAM SHEN

Source apportionment

The concept of *source apportionment* involves identifying sources of air pollution and estimating apportionments of the concentrations of the pollutants observed at various sites in the environment. The results obtained can be used to help manage effectively the quality of the environment.

Receptor-oriented Model

For estimating source apportionment, several receptor-oriented models (*see* **Receptor modeling**) of chemical mass balance (CMB; *see* **Chemical mass balance**) and multivariate statistical methods (**factor analysis**, principal component analysis and so on) have been widely used. See, for example, [1], [2], [5] and [6]. These models are substantially based on the assumption of mass conservation and a mass balance analysis.

Suppose that there are n observations $(x_{i1}, \ldots, x_{ip})$, $i = 1, \ldots, n$, of p elements in the material, where x_{ij} is the concentration ($\mu g\, m^{-3}$) of the jth component in the ith sample. If there are m ($< p$) possible sources, then the *general receptor-oriented model* can be expressed as

$$x_{ij} = \sum_{k=1}^{m} a_{jk} g_{ki}, \quad i = 1, \ldots, n, \; j = 1, \ldots, p \quad (1)$$